P-ISSN 2586-9000
E-ISSN 2586-9027
Homepage : *https://tcithaijo.org/index.php/SciTechAsia* Science & Technology Asia
Vol. 23 No.2 April - June 2018 Page: [54 – 65]

Original research article

Design of Trajectory Tracking System for DC Motors with Uncertain Time-Varying Inertial Loads

Pinit Ngamsom[1,*]
[1]*Department of Mechanical Engineering,*
Rangsit University, Pathum thani 12000, Thailand

Received 5 February 2018; Received in revised form 6 April 2018
Accepted 24 April 2018; Available online 30 June 2018

ABSTRACT

We considered the problem in which a DC motor was controlled to track a given trajectory when the corresponding driven load was associated with uncertain time-varying mass moment of inertia. With the existence of such inertia variation, the corresponding system matrix and input matrix of the control system were simultaneously uncertain and time-varying. Accordingly, stability of the control system could not be guaranteed by simply locating all the poles of the linearized model in the LHP at all time. Based on Lyapunov stability theorem, we came up with a robust PID controller design technique that yielded satisfactory results for this problem. Our robust PID controller was easy to implement, and guaranteed uniform input-to-state stability for the system. It appeared in our investigation on a large Maxxon DC motor that our controller allowed as high as 100% variation of equivalent inertia loading with respect to rotor inertia. We provided a tool to facilitate controller tuning so that the resulting control signal stayed within practical bounds, while achieving a satisfactory level of performance. By selecting an appropriate transmission ratio, our tracking control system could be employed in demanding applications such as independent joint control of robots, and spindle control of modern machining machines.

Keywords: robot; stability; robustness; trajectory tracking; PID; loading variation; inertia variation

1. Introduction

DC motors are actuators that we often find in many demanding machines such as modern machining equipment, including various types of robots. They are actuators of choice in low-to- medium power applications. Their simple structures and principle of operations allow relatively easy and economical designs of controllers and amplifiers. With advances in manufacturing processes, DC motors with efficiency in a

***Corresponding author:** ngamsomp@hotmail.com **doi:** 10.14456/scitechasia.2018.15

range of 85% - 90% are readily available in the market at reasonable prices [1]. Accordingly, research on DC motor control systems has been produced steadily. Indeed, intelligent controller design techniques such as neural networks [2], fuzzy logic [3-6], and genetic algorithm [7] have been applied to the problem of interest. With applications of these techniques, the resulting control systems could be nonlinear and time-varying. In this situation, convergence of trajectories deduced from numerical simulation results does not necessarily imply stability of the control systems. Indeed, there could be some initial conditions from which trajectories diverge from the origin.

Sliding-mode control was applied to DC motors and exceptional performance was demonstrated by means of numerical simulations [8]. However, switching of the control signal in accordance with the associated sliding surfaces caused output chattering and a very large control signal, which could be unacceptable and very difficult to implement. In [9], chattering was handled by introducing a boundary layer to the associated sliding surface. However, such undesirable characteristics could hardly be avoided in practice. Conventional controller design techniques such as LQR and PID, which could guarantee asympotic stablity for linear DC motor control systems, can be found in [10-12]. References [13-14] give introductory reviews of various DC motor control systems. These include conventional controller design techniques such as PI, PD, PID, and LQR, as well as intelligent controller design techniques such as fuzzy logic, and genetic algorithm. In all of the above works, the mass moment of inertia of the load driven by the motor was fixed. While this is a reasonable assumption in many basic cases, it is not so in several demanding cases. For robots with revolute joints, or machines that involve rotation of objects with different masses and shapes, the associated DC motor control system should be able to handle variations of mass moment of inertia.

In this paper, we consider the problem of trajectory tracking control for a DC motor in which mass moment of inertia of the driven object could vary to a significant degree. Our PID control system offers a theoretical guarantee of input-to-state stability. In addition to being easy to implement, it is free from chattering and requires a practical magnitude of control signal.

2. Mathematical Models

Consider the schematic in Fig. 1, in which a DC motor is employed to drive an object via a transmission gearbox. We denote by J_M and J_L, mass moment of inertia of motor rotor and of the loading object, respectively. Note that these values are taken about the relevant rotational axes. The rotor and the loading object are joined by a transmission gearbox with transmission ratio r_T. For convenience, we include mass moment of inertia of the transmission with J_L. Other relevant parameters of the motor are given in Table 1.

Table 1. Notations for relevant parameters of DC motor

Symbol	Meaning
R	terminal resistance (Ohm)
L	terminal inductance (Henry)
K_T	torque constant (N.m/A)
K_b	speed constant (rad/(V.s))
b_M	coefficient of viscous moment for rotor (N.m.s/rad)

A standard mathematical model of the motor is well known, and could be found in the literature. However, we provide it here for convenience of the readers:

$$J_M\ddot{\theta}_M + b_M\dot{\theta}_M = T_M - T_G \tag{2.1}$$

$$V - K_b\dot{\theta}_M = iR + L\left(\frac{di}{dt}\right) \tag{2.2}$$

where V is motor control voltage (Volt), i is armature current (A), is rotational angle of the rotor (rad), is motor torque produced by the flow of electrical current in the armature (N.m), and is the torque applied to the transmission by the motor (N.m). It is typical for DC motors that L is very small when compared to R and . As an example, it is listed in [1] for DC motor model RE65 with part number 353297 that L = H, R = 0.365 Ohm, and rad/(V.s). Because of this, it is reasonable to simplif Eq. (2.2) to obtain:

$$V - K_b\dot{\theta}_M = iR \qquad (2.3)$$

For the transmission, we have the following equation:

$$r_T = \frac{\theta_M}{\theta_L} = \frac{T_L}{\eta_T T_G} \qquad (2.4)$$

where θ_L is rotational angle of the loading object (rad), T_L is the torque applied to the object by the transmission (N.m), and η_T is the efficiency of mechanical transmission. Typically, we have that $0 < \eta_T < 1$, and η_T tends to get small when r_T gets large [1].

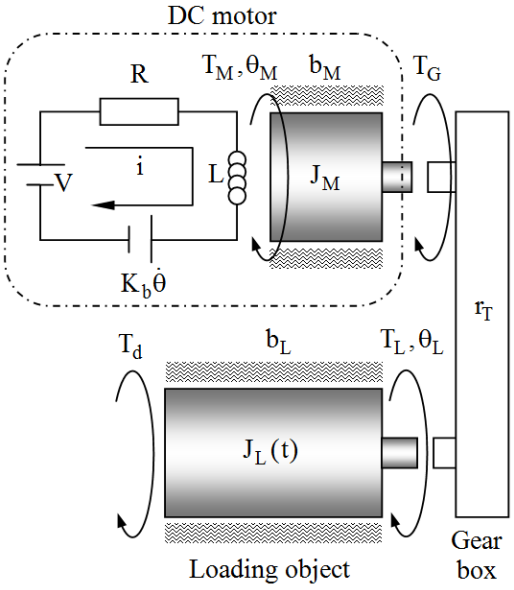

Fig. 1 Schematic of DC Motor with Transmission Gear Box and Loading Object

Normally, the mass moment of inertia of the transmission gearbox, denoted by J_T, is small when compared to that of the loading object. Accordingly, we simply treated it as a part of J_L, the mass moment of the inertia of the object about its axis of rotation. For the loading object, we simply have:

$$J_L\ddot{\theta}_L + b_L\dot{\theta}_L = T_L + T_d \qquad (2.5)$$

where b_L is coefficient of viscous moment for the loading object (N.m.s/rad), and T_d is disturbance torque applied to it. It is straightforward to show that Eq. (2.1), (2.4) and (2.5) may be combined to obtain:

$$\left(J_M + \frac{J_L}{\eta_T r_T^2}\right)\ddot{\theta}_M + \left(b_M + \frac{b_L}{\eta_T r_T^2}\right)\dot{\theta}_M = T_M + \left(\frac{1}{\eta_T r_T}\right)T_d \qquad (2.6)$$

To account for demanding situations in which the loading object could change drastically, we allow J_L to be uncertain and time-varying such that the ratio $J_L/(\eta_T r_T^2)$ could be as large as J_M. It is clear that, depending on r_T, this parameterization could allow very large variation for J_L with respect to J_M. We require, however, that $J_L(t)$ is uniformly globally Lipschitz. We now write Eq.(2.6) as:

$$J_E\ddot{\theta}_M + b_E\dot{\theta}_M = K_T i + \left(\frac{1}{\eta_T r_T}\right)T_d \qquad (2.7)$$

where we substitute $T_M = K_T i$, and denote $J_E \equiv J_M + (J_L/(\eta_T r_T^2))$, $b_E \equiv b_M + (b_L/(\eta_T r_T^2))$. Because we allow the variation of parameter $J_L/(\eta_T r_T^2)$ to be as large as J_M, it then follows that $2J_M \geq J_E > J_M$. We solve Eq. (2.3) for i, and substitute the result in Eq. (2.7) to obtain:

$$\ddot{\theta}_M = -\left(\frac{K_T K_b}{RJ_E} + \frac{b_E}{J_E}\right)\dot{\theta}_M + \left(\frac{K_T}{RJ_E}\right)V + \left(\frac{1}{\eta_T r_T J_E}\right)T_d \quad (2.8)$$

For our DC motor trajectory tracking control system, we want θ_M to track a time-varying reference trajectory θ_R. The corresponding tracking error is defined as $e = \theta_R - \theta_M$, and it follows that $\dot{e} = \dot{\theta}_R - \dot{\theta}_M$, and $\ddot{e} = \ddot{\theta}_R - \ddot{\theta}_M$. We substitute $\ddot{\theta}_M = \ddot{\theta}_R - \ddot{e}$, and $\dot{\theta}_M = \dot{\theta}_R - \dot{e}$ in Eq. (2.8), and solve for $\ddot{e}$ to obtain:

$$\begin{aligned}\ddot{e} = &-\left(\frac{K_T K_b}{RJ_E} + \frac{b_E}{J_E}\right)\dot{e} - \left(\frac{K_T}{RJ_E}\right)V \\ &-\left(\frac{1}{\eta_T r_T J_E}\right)T_d + \ddot{\theta}_R + \left(\frac{K_T K_b}{RJ_E} + \frac{b_E}{J_E}\right)\dot{\theta}_R\end{aligned} \quad (2.9)$$

We now define three state variables: $x_1 \equiv \int e\,dt$, $x_2 \equiv e$, and $x_3 \equiv \dot{e}$. The corresponding state vector is $x = [x_1 \quad x_2 \quad x_3]^T$. Error dynamics of the trajectory tracking control system can now be written in vector-matrix form:

$$\dot{x} = A_T x + B_T V + N T_d + H\dot{\theta}_R + W\ddot{\theta}_R \quad (2.10)$$

where $A_T = \begin{bmatrix} 0 & 1 & 0 \\ 0 & 0 & 1 \\ 0 & 0 & -\frac{K_T K_b}{RJ_E} - \frac{b_E}{J_E} \end{bmatrix}$,

$B_T = \begin{bmatrix} 0 \\ 0 \\ -\frac{K_T}{RJ_E} \end{bmatrix}$, $N = \begin{bmatrix} 0 \\ 0 \\ -\frac{1}{\eta_T r_T J_E} \end{bmatrix}$,

$H = \begin{bmatrix} 0 \\ 0 \\ \frac{b_E}{J_E} + \frac{K_T K_b}{RJ_E} \end{bmatrix}$, and $W = \begin{bmatrix} 0 \\ 0 \\ 1 \end{bmatrix}$

Eq. (2.10) is used for our trajectory tracking control system design. For this, we assign a PID control law to the input voltage V such that $V = -Kx$, where $K = [k_1 \quad k_2 \quad k_3]$ is the state- feedback gain matrix. Clearly, the control law is linear and free from chattering. Our design objective is to find K such that input-to-state stability [15] of the system is theoretically guaranteed when the time-varying inertia J_E is such that $2J_M \geq J_E > J_M$. Notice that the elements $A_T(3,3)$, $B_T(3,1)$, N(3,1), and H(3,1) can be twice as large when J_E changes from $2J_M$ to J_M. By achieving input-to-state stability, we expect that all trajectories will converge to the origin when θ_R and T_d are constant. When θ_R and T_d are time-varying, all trajectories stay in a small neighborhood about the origin.

Recall that Eq. (2.10) is obtained by simplifying Eq. (2.3), using the fact that L is very small when compared to R and K_b. Because of this, di/dt does not appear in Eq. (2.10). This is useful for controller design because it reduces the order of the control system by one. In addition, it removes necessity of using i as a feedback signal. After an appropriate stabilizing gain K is found, however, one may want to investigate how the original system performs with the resulting control law. It turns out that mathematical description of the original system has the same structure as Eq. (2.10), but with the relevant matrices being:

$$A_T = \begin{bmatrix} 0 & 1 & 0 & 0 \\ 0 & 0 & 1 & 0 \\ 0 & 0 & -\frac{b_E}{J_E} & -\frac{K_T}{J_E} \\ 0 & 0 & \frac{K_b}{L} & -\frac{R}{L} \end{bmatrix},\ B_T = \begin{bmatrix} 0 \\ 0 \\ 0 \\ \frac{1}{L} \end{bmatrix},$$

$$H = \begin{bmatrix} 0 \\ 0 \\ \frac{b_E}{J_E} \\ -\frac{K_b}{L} \end{bmatrix},\ N = \begin{bmatrix} 0 \\ 0 \\ -\frac{1}{\eta_T r_T J_E} \\ 0 \end{bmatrix},\ W = \begin{bmatrix} 0 \\ 0 \\ 1 \\ 0 \end{bmatrix}, \text{ and}$$

$$x = \begin{bmatrix} x_1 \\ x_2 \\ x_3 \\ x_4 \end{bmatrix}$$

where $x_4 \equiv i$. At this point, mathematical models of our trajectory tracking control system are already written in a form that facilitates controller design. This is addressed in the next section.

3. Controller Design

Consider the mathematical model of a linear uncertain time-varying system shown in Eq. (3.1):

$$\dot{x} = [A + \Delta A(t)]x + [B + \Delta B(t)]u + w(t) \quad (3.1)$$

where $x \in \Re^n$ is the state vector, the nominal system matrix $A \in \Re^{n\times n}$ is known, the nominal input matrix $B \in \Re^{n\times m}$ is known, $u \in \Re^m$ is the control input vector, and the bounded time-varying perturbation vector $w(t) \in \Re^n$. Our control system may be described by Eq. (3.1) with n = 3 and m = 1, in which:

$$A = A_T\big|_{J_E = J_M},$$

$$\Delta A = A_T\big|_{J_E = 2J_M} - A_T\big|_{J_E = J_M},$$

$$B = B_T\big|_{J_E = J_M},\ \Delta B = B_T\big|_{J_E = 2J_M} - B_T\big|_{J_E = J_M},$$

$$w(t) = NT_d + H\ddot{\theta}_R + W\dddot{\theta}_R.$$

For now, let us employ the linear state-feedback control law $u = -Kx$, in which $K \in \Re^{m\times n}$ is a constant gain matrix such that $\bar{A} = A - BK$ is Hurwitz. When all the associated bounds for the time-varying elements are known, and the perturbation vector w(t) is removed from Eq. (3.1), we can always write:

$$\dot{x} = \bar{A}x + \sum_{j=1}^{N}[h_j(t)E_j]x \quad (3.2)$$

where $E_j \in \Re^{n\times n}$ is known, and $h_j(t) \in \Re$ is a time-varying function with known strict upper bound $h_{uj} > h_j$ and strict lower bound $h_{lj} < h_j$. We say that K is a stabilizing solution if it guarantees uniform global exponential stability of the equilibrium point at the origin of Eq. (2.5). Theorem 1 [16] gives a sufficient condition for a stabilizing solution of single-input cases. It was extended to multiple-input cases in [17]. The latter is provided here for convenience of the reader.

Theorem 1 If the dynamical system in Eq. (3.2) is uniformly globally Lipschitz with $\bar{A}$ being Hurwitz and $\max(\lambda(Z)) < 0$, then the equilibrium point at the origin is uniformly globally exponentially stable. The matrix $Z = Z^T \in \Re^{n\times n}$ is obtained by:

1) Specified $Q > 0$ and $\bar{A}$ to compute P from the Lyapunov equation $-Q = (1/2)[P\bar{A} + \bar{A}^T P]$
2) Compute $\bar{A}_l = \bar{A} + \sum_{j=1}^{N} h_{lj}E_j$ and $\Phi = P\bar{A}_l + \bar{A}_l^T P$.
3) Compute $\Psi_j = [PE_j + E_j^T P] = \Psi_j^T \ \ \forall j$.
4) Compute $\Lambda_{\Psi_j} = T_{\Psi_j}^T \Psi_j T_{\Psi_j} = \mathrm{diag}[\lambda_{\Psi_j 1} \ \dots \ \lambda_{\Psi_j n}] \quad \forall j$, where $T_{\Psi_j} = [v_{\Psi_j 1} \mid \dots \mid v_{\Psi_j n}]$, $\{v_{\Psi_j 1}, \dots, v_{\Psi_j n}\}$ is the set of n orthogonal unit (orthonormal) eigenvectors of Ψ_j, and $\{\lambda_{\Psi_j 1}, \dots, \lambda_{\Psi_j n}\}$ is the corresponding set of n real eigenvalues of Ψ_j.

5) Set all negative elements of Λ_{Ψ_j} to zero to get $\Lambda_{\Psi_j}^{\geq 0} \quad \forall j$.

6) Compute $\Psi_j^{\geq 0} = T_{\Psi_j} \Lambda_{\Psi_j}^{\geq 0} T_{\Psi_j}^T \quad \forall j$.

7) Compute $Z \equiv \Phi + \sum_{j=1}^{r} [(h_{uj} - h_{lj}) \Psi_j^{\geq 0}]$.

Proof See [17].

In our control system, the perturbation vector w(t) vanishes only when $T_d = 0$ and θ_R is constant. Clearly, these conditions do not hold in general practices. With existence of w(t), [17] shows that trajectories converge into a neighborhood about the origin. The size of this neighborhood is in accordance with that of the perturbation vector. This is a type of stability known as input-to-state stability [15].

Using Theorem 1, [17] proposes a procedure for generating K using two controller design parameters ρ and η without relying on the exact expressions of $h_j(t)$. Although it appears that the procedure can give satisfactory results when compared to those from existing controller design techniques, it primarily addresses robust stabilization only. While robust stability is probably the most important property of any control systems, there are additional properties of lower importance that should also be considered. In particular, the control law should not demand an excessively large control signal because this could be too expensive to implement and to operate. In this paper, we extend the use of Theorem 1 to obtain a 2D chart for tuning the resulting linear control law. This allows one to conveniently obtain preferable balances between performance, and magnitude control signal, while maintaining robust stability. The procedure in [17] is revised to include this feature in this section. There are two phases in the revised controller design procedure. In the first phase, an additional layer of optimization is incorporated to find a stabilizing solution K. It appeared in our investigation that this could significantly reduce conservatism of allowable uncertainty bounds on $h_j(t)$. The second phase involves tuning of the stabilizing solution K found in the first phase. The first phase can be fully automated in a computer, while the second phase usually requires designer experiences.

Phase I (Robust Stabilization)

1) Define a two dimensional domain of $\rho > 0$ and $\eta \geq 1$, and select a grid size for this domain.
2) Select a diagonal matrix $\hat{Q} > 0$. An initial choice of $\hat{Q} = I$ often leads to a stabilizing solution. For each coordinate of (ρ, η), execute the following steps 3) – 5)
3) Solve for P from the equation:

$$-2\hat{Q} = PA + A^T P - 2\rho PBB^T P \qquad (3.3)$$

The existence of a unique solution $P > 0$ is guaranteed [18].

4) Compute a stabilizing gain matrix candidate:

$$K = \eta \rho B^T P \qquad (3.4)$$

Then $\bar{A} \equiv A - BK$, and $Q = -(1/2)[P\bar{A} + \bar{A}^T P]$. The matrix $\bar{A}$ is guaranteed to be Hurwitz [18].

5) Use ($\bar{A}$, Q) obtained in step 3) to compute Z by executing steps 2) – 7) in Theorem 1.
6) If $\max(\lambda(Z)) < 0$ at a particular coordinate of (ρ, η), then corresponding K is a stabilizing solution and phase I terminates successfully. Otherwise, employ the univariate optimization on each element of $\hat{Q}$ and repeat steps 3) – 5).

Phase II (Controller Tuning)

When the procedure in Phase I terminates successfully, we obtain the stabilizing gain matrix $K = \eta \rho B^T P$. Because B is given by the mathematical model, we see that K depends on P. Additionally, ρ is the design parameter that we employ to determine P by solving Eq. (3.4). In general, Eq. (3.4) is solved

numerically. Accordingly, the influence of ρ on certain properties of K is not clear. These include proportion of the elements of K, and magnitude of K. Because of this, ρ is not a good candidate for tuning the controller by hand. On the contrary, it is clear that increasing η increases the magnitudes of the elements of K without altering their proportions. It appears in our investigations that this property is useful for tuning K to find a preferable balance between system performance and magnitude control signal, while maintaining robust stability obtained in Phase I.

To do this, we plot η against $\max(\lambda(Z))$ at a certain value for ρ when $\max(\lambda(Z)) < 0$ for some values of η, and select $\eta = \eta^*$ that corresponds to such a preferable balance. In general, we can increase performance by increasing η. However, this comes at a price of large K matrices and thus large control signals, which could prohibit applications of the resulting control laws in practices.

For various sets of realistic design data, it took us no greater than a minute to complete Phase I for each set of data on a PC with Core2 CPU. For Phase II, it depends largely on designer experience and preference, as well as constraint on magnitude of control signal and desired level of performance. This is shown in the next section.

4. A Numerical Design Example

Consider a trajectory tracking control system design in which a Maxon DC motor model 353297 is employed to drive an unknown loading object. Relevant parameters of the motor are shown in Table 2.

Table 2. Relevant design parameters for Maxon DC motor model 353297

Parameter	Value
R	0.365 Ohm
L	0.161×10^{-3} Henry
K_T	0.123 N.m/A
K_b	$K_b = 8.15$ rad/(V.s)
b_M	NA
J_M	1340×10^{-7} kg.m^2
Nominal Torque	0.8 N.m
Nominal Voltage	48 V

The associated transmission gearbox joining the motor and the loading object is Maxon part no. 223085, whose relevant design parameters are shown in Table 3.

Table 3. Relevant design data for Maxon transmission gear box part no. 223085

Parameter	Value
r_T	19
η_T (max)	0.83 (i.e., 83%)
J_T	9.5×10^{-7} kg.m^2

The control system is supposed to operate in unpredictable environments in which mass moment of inertia J_L of the loading objects and disturbance torque T_d are unknown and could change continuously. Recall that our design objective is such that $J_L/(\eta_T r_T^2) \le J_M$. This translates to allowable variation of the inertia ratio $(J_L/J_M) \le \eta_T r_T^2 = 299.3$. Accordingly, we allow J_L to be uncertain and time-varying but it should not be larger than $299.3\,J_M$ (i.e., 0.4 kg.m^2). Notice that J_T is indeed very much smaller than the maximum value of J_L.

To obtain the feedback gain matrix K, our controller design technique requires availability of matrices A, B, ΔA, and ΔB in the mathematical model of Eq. (3.1). Using the parameters in Tables (2-3), we obtain:

$$A = \left[\begin{array}{c|c|c} 0 & 1 & 0 \\ \hline 0 & 0 & 1 \\ \hline 0 & 0 & -20489.5 \end{array}\right],\ \Delta A = \left[\begin{array}{c|c|c} 0 & 1 & 0 \\ \hline 0 & 0 & 1 \\ \hline 0 & 0 & h_1(t) \end{array}\right],$$

$$B = \begin{bmatrix} 0 \\ 0 \\ -2514.82 \end{bmatrix}, \quad \Delta B = \begin{bmatrix} 0 \\ 0 \\ h_2(t) \end{bmatrix}$$

where all we know about $h_1(t)$, and $h_2(t)$ is that they are not negative and are bounded by 10244.75, and 1257.41, respectively. Following the procedure given in Section 3, it takes approximately 2 seconds for a PC with Core 2 Duo CPU to generate a 3D graph of design parameters ρ and η versus $\max \lambda(Z(\rho,\eta))$ when $\hat{Q} = \text{diag}(0.1, 0.1, 0.19)$ as in Fig. (2). It appears from the figure that there are many coordinates of (ρ,η) at which $\max(\lambda(Z(\rho,\eta))) < 0$. We simply choose coordinate $(\rho^*, \eta^*) = (60, 10)$, which corresponds to $\max(\lambda(Z)) = -0.16$, and the stabilizing gain matrix:

$$K = \begin{bmatrix} -24.49 & -56.49 & -12.17 \end{bmatrix} \qquad (4.1)$$

Note that there are many other choices for $\hat{Q}$ that can be employed to obtain similar results.

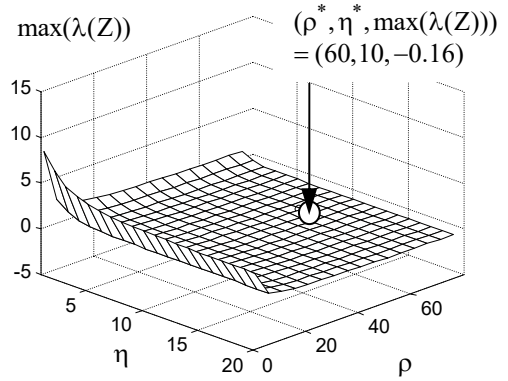

Fig.2. A 3D graph of $\max \lambda(Z(\rho,\eta))$ versus design parameters ρ and η, with the selected pair $(\rho^*, \eta^*) = (60, 10)$ marked by a sphere

Bahavior of the resulting control system is now investigated using numerical simulations. For this, we invoke the original 4-th order dynamic system with terminal inductance L. The reference trajectory used in our investigation is:

$$\theta_R = \begin{cases} 10\sin(t) & \text{rad}, \ 0 \le t < 6 \\ 10 & \text{rad}, \ 6 \le t \le 10 \end{cases}$$

and $J_L(t) = 0.5 J_M \eta_T r_T^2 (1 + \sin(t)\cos(t))$. Notice that this uncertain time-varying inertia yields $J_E(t) = J_M + 0.5 J_M (1 + \sin(2t)\cos(t))$, which conforms with our design specification that $2J_M \ge J_E > J_M$. In addition to this, the control system is also tested with a cyclical disturbance torque of $T_d(t) = 10\,\text{sign}(\sin(2t))$ N.m, which is known only after the system is put into operation. Note that $J_L(t)$ is shown in Fig. 3, and $T_d(t)$ is shown in Fig. 4. Reference trajectory θ_R, and actual trajectory θ_M are also shown in Fig. 4, from which we see that θ_M tracks θ_R closely as desired.

Fig. 5 shows tracking error $x_1 = e$ and derivative of tracking error $x_2 = \dot{e}$. It appears that both are loosely bounded by ± 1.8 rad during the first 6 seconds, in which θ_R varies with time. They reduce quickly to a very small value after 6 seconds when θ_R is fixed at 10 rad. Small spikes of x_2 in Fig. 5 are associated with abrupt changes of $T_d(t)$ between 10 and -10 N.m. The controller is able to suppress these spikes very quickly. Notice that the system responses show no chattering.

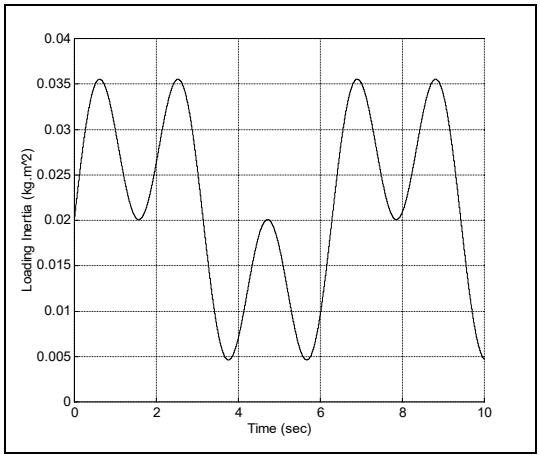

Fig.3. Polar mass moment of inertia of loading object versus time

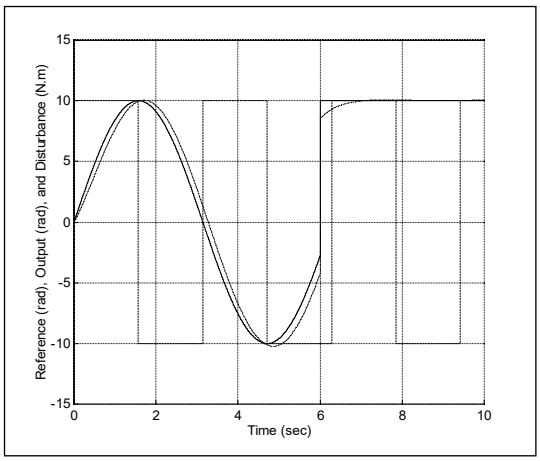

Fig.4. Reference trajectory $\theta_R(t)$ (solid: rad), motor trajectory $\theta_M(t)$ (dash-dot: rad), and disturbing torque T_d (dash square wave: N.m)

The control voltage V(t) is shown in Fig. 6. We see that, except at the instances that $T_d(t)$ changes abruptly, the control voltage is smooth at all time. Notice that V(t) is less than the motor nominal voltage of 48 V for most of the time. This behavior is necessary for the motor to operate continuously without overheating. In general, it appeared in our investigation that the tracking error could be much smaller when large values for η were chosen to obtain K. However, this also enlarged all the elements of K in Eq. (3.6) proportionally, and led to V(t) being much higher than the nominal voltage of the motor. To explore this, consider the plot of η versus the maximum value of $\lambda(Z)$ provided in Fig. 7 with ρ being fixed at $\rho^* = 60$.

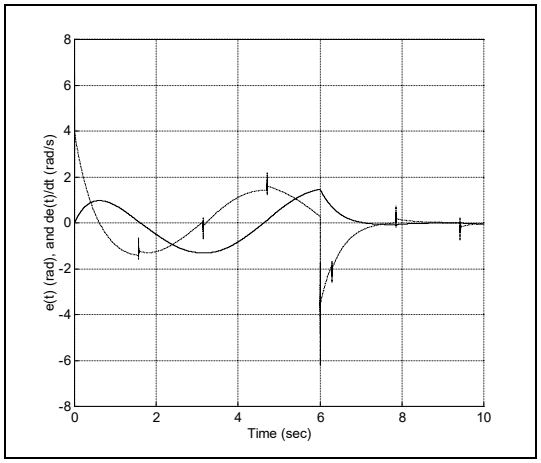

Fig.5. Tracking error $e(t) = x_2(t)$ (solid: rad), and $\dot{e}(t) = x_3(t)$ (dash-dot: rad/s) with $\eta = 10$

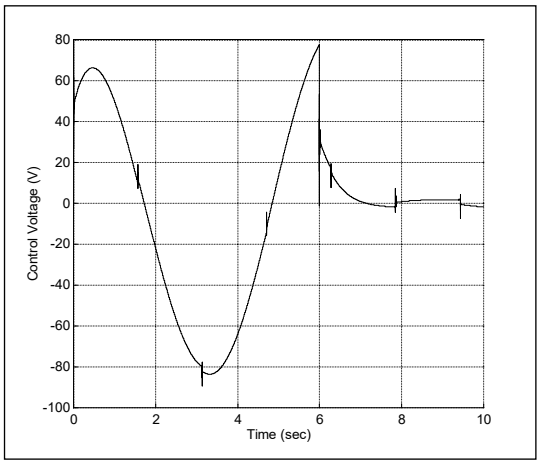

Fig.6. Control voltage V(t) (Volt) with $\eta = 10$

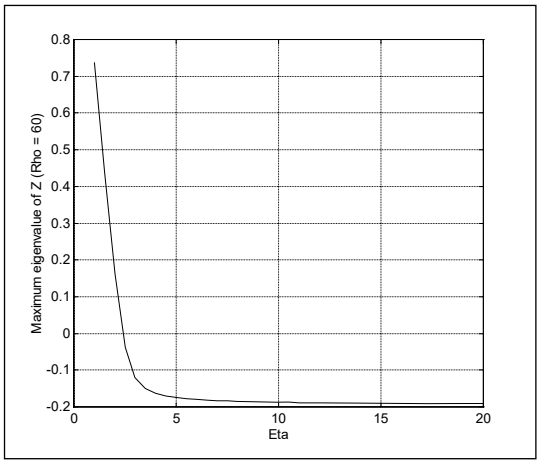

Fig.7. Maximum of $\lambda(Z)$ versus η when $\rho = 60$

The fact that max $(\lambda(Z))$ < 0 when $\eta = 10$ implies that our control system allows J_L to be larger than $299.3\, J_M$. We do not pursue this because we have already met our objective. Fig. 7 also suggests that we can use $\eta > 10$ to enlarge K and enhance performance, while preserving robust stability. This, however, decreases max $(\lambda(Z))$ very little and thus hardly improves robustness of the control system.

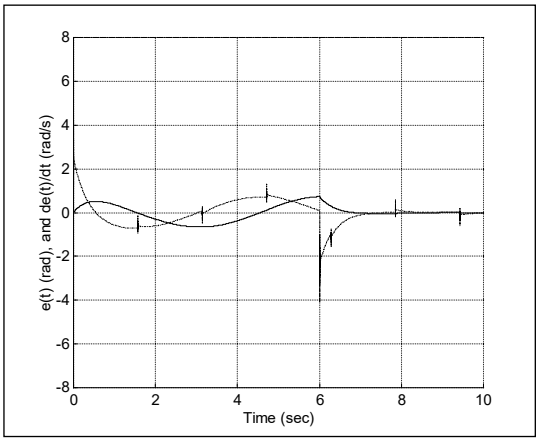

Fig.8. Tracking error $e(t) = x_2(t)$ (solid: rad), and $\dot{e}(t) = x_3(t)$ (dash-dot: rad/s) with $\eta = 20$

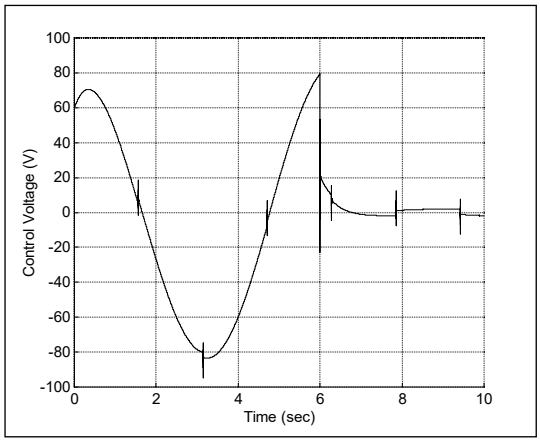

Fig.9. Control voltage V(t) (Volt) with $\eta = 20$

Now, let us examine effects of using $\eta = 20$. Clearly, the corresponding stabilizing gain matrix K is larger than that in Eq. (4.1) by 100%. Fig. 8 depicts the resulting tracking error, which is now bounded by ±1 rad. This is approximately 55% smaller than that when $\eta = 10$. The associated control voltage is shown in Fig. 9. We see that it is generally larger than that when $\eta = 10$, but the difference is less than 10% approximately. At this point, we have demonstrated the use of our controller tuning tools. It is up to a designer to weight system performance against maximum magnitude of the corresponding control voltage, and select an appropriate balance for the control system of interest.

5. Conclusion

For demanding applications such as independent joint control of robots and spindle control of advanced machining equipment, the associated DC motors could constantly be subjected to variation of mass moment of inertia of loading objects. In this paper, we derived a mathematical setup that could be used to facilitate design of PID controllers for trajectory tracking of DC motors subjected to uncertain time-varying inertia of loading objects. Then, we discussed a revised controller design technique for the

class of dynamic systems of interest. The revised technique was composed of two phases. The first phase primarily focused on guaranteed robust stability of the resulting control system. In the second phase, the objective was to tune the controller obtained from the first phase. For this, we propose a 2D chart that could be employed to find balances between performance of the control system and the required magnitude of control voltage, while preserving robust stability. This chart was distinctly easy to use and offered immediate interpretation for tuning action. Using sets of realistic data for the system of interest, it appeared that the resulting controller could guarantee input-to-state stability when inertia of the loading object varied significantly. In addition, it could be designed to operate in a safe zone of control voltage and yield a satisfactory level of performance simultaneously.

References

[1] Maxon Motor AG., Selection Guide: program 2017/2018, Switzerland, 2017.

[2] Amit Atri, and Md. Ilyas, Speed control of DC motor using neural network configuration, International Journal of Advanced Research in Computer Science and Software Engineering, Vol. 2, Issue 5, pp. 209-212, May 2012.

[3] Abdulrahman A. A. Emhemed and Rosbi Bin Mamat, Modelling and simulation for industrial DC motor using intelligent control, International Symposium on Robotics and Intelligent Sensors, pp. 420-425, 2012.

[4] Jaydeep Chakravorty, and Ruchika Sharma, Fuzzy logic based method of speed control of DC motor, International Journal of Emerging Technology and Advanced Engineering, Vol. 3, Issue 4, pp. 64-66, April 2013.

[5] Ravinder Kumar, and Vineet Girdha, High performance fuzzy adaptive control for DC motor, Global Journal of Researches in Engineering, Vol. 3, Issue 10, 2013.

[6] Meysam Shadkam et. al., Speed control of DC motor using extended Kalman filter based fuzzy PID, International Journal of Information and Electronics Engineering. Vol. 3, No. 1, pp. 109-112, January 2013.

[7] Esmaeil Saneni et. al., Design of optimal PID control of DC motor using genetic algorithm, International Journal of Computer Theory and Engineering, Vol. 4, No. 3, pp. 433-435 June 2012.

[8] Emre Hasan Dursun, and Akif Durdu, Speed control of a DC motor with variable load using sliding mode control, International Journal of Computer and Electrical Engineering, Vol. 8, No. 3, June 2016.

[9] Arun Prasad K. M. et. al., Modified chattering free sliding model control of DC motor, International Journal of Modern Engineering Research, Vol. 3, Issue 3, pp. 1419-1423, May 2013.

[10] Saisudha V. et. al., Analysis of speed control of DC motor using LQR method, International Journal of Control Theory and Applications, pp. 7377-7385, 2016.

[11] Ramesh K et al. Design of current controller for two quadrant DC motor drive by using model order reduction technique. International Journal of Computer Science and Information Security 2010; 7: 1: 17-24.

[12] Aditya PS et al. Speed control of DC motor using PID controller based on MATLAB. Innovative Systems Design and Engineering 2013; 4: 6: 22-28.

[13] Nikhil T et al. Analysis of speed control of DC motor – a review study. International Research Journal of Engineering and Technology 2015; 2: 8: 1616-1621.

[14] Vijay S, Vijay KG. A comparative study on speed control of DC motor using intelligent techniques. International Journal of Electronics and Electrical Engineering 2014; 7: 4: 431-436.

[15] Hassan KK. Nonlinear systems. 3rd edition: Prentice Hall: New Jersey; 2000.

[16] Pinit N, Larry LH. Using robust stability analysis theorems for robust controller design. ASME Journal Of Dynamic Systems, Measurement, and Control 2003; 125: 4: 669-671.

[17] Pinit N. A graphical robust PID controller design for time-varying uncertain systems with applications to trajectory tracking of a load-varying rigid SCARA. Thammasat International Journal of Science and Technology 2016; 21: 2: 34-44.

[18] Wassim MH, Vijay SC. Nonlinear dynamical systems and control: a Lyapunov-based approach. Princeton University Press; 2008.